

## MODEL TO SIMULATE THE BEHAVIOUR OF RC BEAMS SHEAR STRENGTHENED WITH ETS BARS

JOAQUIM BARROS<sup>\*</sup>, MATTEO BREVEGLIERI<sup>†</sup>, ANTÓNIO VENTURA-GOUVEIA<sup>+</sup>,  
GLAUCIA DALFRE<sup>\*</sup>, AND ALESSANDRA APRILE<sup>†</sup>

<sup>\*</sup> University of Minho  
ISISE, University of Minho, Guimarães, Portugal  
e-mail: barros@civil.uminho.pt, gmdalfre@civil.uminho.pt

<sup>+</sup> Polytechnic Institute of Viseu  
ISISE, School of Technology and Management of Viseu, Viseu, Portugal  
e-mail: ventura@estv.ipv.pt

<sup>†</sup> University of Ferrara  
Engineering Department, Via Saragat 1, Ferrara, Italy  
e-mail: matteo.breveglieri@unife.it, prllsn@unife.it

**Keywords:** Shear strengthening, Reinforced concrete, ETS technique, Analytical model, FEM simulations.

**Abstract:** To predict correctly the deformational and the cracking behavior of reinforced concrete elements failing in shear using a smeared crack approach, the strategy adopted to simulate the crack shear stress transfer is crucial. For this purpose, several strategies for modeling the fracture mode II were implemented in a smeared crack model already existing in the FEM-based computer program, FEMIX. Special development was given to a softening shear stress-shear strain diagram adopted for modeling the crack shear stress transfer.

The predictive performance of the implemented constitutive model was assessed by simulating up to failure a series of eight beams tested to appraise the effectiveness of a new strengthening technique to increase the shear resistance of reinforced concrete beams. According to this strengthening technique, designated as Embedded Through-Section (ETS), holes are opened through the beam's section, with the desired inclinations, and bars are introduced into these holes and bonded to the concrete substrate with adhesive materials. The strengthening elements are composed of steel bars bonded to the surrounding concrete with an epoxy adhesive.

By using the properties obtained from the experimental programs for the characterization of the relevant properties of the intervening materials, and deriving from inverse analysis the data for the crack shear softening diagram, the simulations carried out have fitted with high accuracy the deformational and cracking behavior of the tested beams, as well as the strain fields in the reinforcements. The constitutive model is briefly described, and the simulations are presented and analyzed.

### 1 INTRODUCTION

Available research shows that the predictive performance of computer programs based on the finite element method (FEM) and incorporating constitutive models for the

material nonlinear analysis of reinforced concrete (RC) structures failing in shear is quite dependent on the constitutive model adopted to simulate the shear stress transfer in the cracked concrete [1]. Recently a total crack shear stress-shear strain approach was

implemented in a multi-directional fixed smeared crack model for a better simulation of the strengthened beams failing in shear and in flexural/shear [2]. This approach was able of simulating the decrease of the total crack shear stress with the crack opening, but the stiffness predicted by the model for the behaviour of some beams was higher than the one registered experimentally. Furthermore, due to numerical instabilities some simulations were not capable of attaining the deflection corresponding to the peak load. In this paper a softening diagram is proposed for modelling the sliding component of the crack constitutive law, and it was implemented into a multi-directional fixed smeared crack model for capturing with high accuracy, not only the deformational and load carrying capacity of reinforced concrete beams failing in shear, but also the crack patterns formed during the loading process of this type of structural elements. To appraise the predictive performance of this model, it was applied on the simulation of the experimental tests carried out with a series of RC beams shear strengthened according to the embedded through-section (ETS) technique. This technique consists on opening holes across the depth of the beams cross section, with the desired inclinations, where bars are introduced and are bonded to the concrete substrate with adhesive materials [3]. The constitutive model is briefly described in this paper, the shear strengthening effectiveness of the ETS technique is demonstrated based on the obtained results, and the predictive performance of the proposed model is assessed by simulating the experimental tests.

## 2 NUMERICAL MODEL

Under the framework of the finite element analysis, the tested beams are considered as a plane stress problem. The description of the formulation of the multi-directional fixed smeared crack model is restricted to the case of cracked concrete, at the domain of an integration point (*IP*) of a plane stress finite element. According to the adopted constitutive law, stress and strain are related by the following equation.

$$\Delta \underline{\sigma} = \underline{D}^{crco} \Delta \underline{\varepsilon} \quad (1)$$

being  $\Delta \underline{\sigma} = \{\Delta \sigma_1, \Delta \sigma_2, \Delta \tau_{12}\}^T$  and  $\Delta \underline{\varepsilon} = \{\Delta \varepsilon_1, \Delta \varepsilon_2, \Delta \gamma_{12}\}^T$  the vectors of the incremental stress and incremental strain components. Due to the decomposition of the total strain into an elastic concrete part and a crack part,  $\Delta \underline{\varepsilon} = \Delta \underline{\varepsilon}^{co} + \Delta \underline{\varepsilon}^{cr}$ , in equation (1) the cracked concrete constitutive matrix,  $\underline{D}^{crco}$ , is obtained with the following equation [4]

$$\underline{D}^{crco} = \underline{D}^{co} - \underline{D}^{co} \left[ \underline{T}^{cr} \right]^T \left( \underline{D}^{cr} + \underline{T}^{cr} \underline{D}^{co} \left[ \underline{T}^{cr} \right]^T \right)^{-1} \underline{T}^{cr} \underline{D}^{co} \quad (2)$$

where  $\underline{D}^{co}$  is the constitutive matrix of concrete, assuming a linear behaviour

$$\underline{D}^{co} = \frac{E_c}{1-\nu_c^2} \begin{bmatrix} 1 & \nu_c & 0 \\ \nu_c & 1 & 0 \\ 0 & 0 & \frac{1-\nu_c}{2} \end{bmatrix} \quad (3)$$

being  $E_c$  and  $\nu_c$  the Young's modulus and the Poisson's coefficient of concrete, respectively. In equation (2)  $\underline{T}^{cr}$  is the matrix that transforms the stress components from the coordinate system of the finite element to the local crack coordinate system (a subscript  $\ell$  is used to identify entities in the local crack coordinate system). If  $m$  cracks occurs at an *IP*

$$\underline{T}^{cr} = \left[ \underline{T}_1^{cr} \quad \dots \quad \underline{T}_i^{cr} \quad \dots \quad \underline{T}_m^{cr} \right]^T \quad (4)$$

being the matrix crack orientation of a generic  $i^{th}$  crack defined by

$$\underline{T}_i^{cr} = \begin{bmatrix} \cos^2 \theta_i & \sin^2 \theta_i & 2 \sin \theta_i \cos \theta_i \\ -\sin \theta_i \cos \theta_i & \sin \theta_i \cos \theta_i & \cos^2 \theta_i - \sin^2 \theta_i \end{bmatrix} \quad (5)$$

with  $\theta_i$  being the angle between the  $x_1$  axis and the vector orthogonal to the plane of the  $i^{th}$  crack. In equation (2)  $\underline{D}^{cr}$  is a matrix that includes the constitutive law of the  $m$  cracks

$$\underline{D}^{cr} = \begin{bmatrix} \underline{D}_1^{cr} & \dots & \underline{0} & \dots & \underline{0} \\ \dots & \dots & \dots & \dots & \dots \\ \underline{0} & \dots & \underline{D}_i^{cr} & \dots & \underline{0} \\ \dots & \dots & \dots & \dots & \dots \\ \underline{0} & \dots & \underline{0} & \dots & \underline{D}_m^{cr} \end{bmatrix} \quad (6)$$

with  $\underline{D}_i^{cr}$  being the crack constitutive matrix of the  $i^{th}$  crack

$$\underline{D}_i^{cr} = \begin{bmatrix} D_{I,i}^{cr} & 0 \\ 0 & D_{II,i}^{cr} \end{bmatrix} \quad (7)$$

where  $D_{I,i}^{cr}$  and  $D_{II,i}^{cr}$  represent, respectively, the modulus correspondent to the fracture mode I (normal) and fracture mode II (shear) of the  $i^{th}$  crack. The behaviour of non-completely closed cracks formed in an *IP* is governed by the following relationship

$$\Delta \underline{\sigma}_\ell^{cr} = \underline{D}^{cr} \Delta \underline{\varepsilon}_\ell^{cr} \quad (8)$$

where  $\Delta \underline{\sigma}_\ell^{cr}$  is the vector of the incremental crack stress components in the coordinate system of each of the  $m$  cracks

$$\Delta \underline{\sigma}_\ell^{cr} = \begin{bmatrix} \Delta \sigma_{n,1}^{cr} & \Delta \tau_{nt,1}^{cr} & \dots & \Delta \sigma_{n,i}^{cr} & \Delta \tau_{nt,i}^{cr} & \dots & \Delta \sigma_{n,m}^{cr} & \Delta \tau_{nt,m}^{cr} \end{bmatrix}^T \quad (9)$$

and  $\Delta \underline{\varepsilon}_\ell^{cr}$  is the vector of the correspondent incremental crack strain components

$$\Delta \underline{\varepsilon}_\ell^{cr} = \begin{bmatrix} \Delta \varepsilon_{n,1}^{cr} & \Delta \gamma_{nt,1}^{cr} & \dots & \Delta \varepsilon_{n,i}^{cr} & \Delta \gamma_{nt,i}^{cr} & \dots & \Delta \varepsilon_{n,m}^{cr} & \Delta \gamma_{nt,m}^{cr} \end{bmatrix}^T \quad (10)$$

Using the  $\underline{T}^{cr}$  matrix, the vector of the incremental crack strain components in the finite element coordinate system,  $\Delta \underline{\varepsilon}^{cr}$ , can be obtained from  $\Delta \underline{\varepsilon}_\ell^{cr}$

$$\Delta \underline{\varepsilon}^{cr} = \left[ \underline{T}^{cr} \right]^T \Delta \underline{\varepsilon}_\ell^{cr} \quad (11)$$

and the equilibrium condition

$$\Delta \underline{\sigma}_\ell^{cr} = \underline{T}^{cr} \Delta \underline{\sigma} \quad (12)$$

must be assured. In the present approach, a new crack is arisen in an *IP* when the angle formed between the new crack and the already existing cracks,  $\theta_{new}^{cr}$ , exceeds a certain threshold angle,  $\theta_{th}$  (a parameter of the constitutive model that in general ranges between 30 and 60 degrees [4]).

The crack opening propagation is simulated with the trilinear diagram represented in Figure 1, which is defined by the normalized stress,  $\alpha_i$ , and strain,  $\xi_i$ , parameters that define the transitions points between the linear

segments of this diagram. The ultimate crack strain,  $\varepsilon_{n,u}^{cr}$ , is defined as a function of the parameters  $\alpha_i$  and  $\xi_i$ , fracture energy,  $G_f^I$ , tensile strength,  $f_{ct} = \sigma_{n,1}^{cr}$ , and crack band width,  $l_b$ , as follows [4],

$$\varepsilon_{n,u}^{cr} = \frac{2}{\xi_1 + \alpha_1 \xi_2 - \alpha_2 \xi_1 + \alpha_2} \frac{G_f^I}{f_{ct} l_b} \quad (13)$$

being  $\alpha_1 = \sigma_{n,2}^{cr} / \sigma_{n,1}^{cr}$ ,  $\alpha_2 = \sigma_{n,3}^{cr} / \sigma_{n,1}^{cr}$ ,  $\xi_1 = \varepsilon_{n,2}^{cr} / \varepsilon_{n,u}^{cr}$  and  $\xi_2 = \varepsilon_{n,3}^{cr} / \varepsilon_{n,u}^{cr}$ . To simulate the fracture mode II modulus,  $D_{II}^{cr}$ , a shear retention factor is currently used [4, 5]:

$$D_{II}^{cr} = \frac{\beta}{1 - \beta} G_c \quad (14)$$

where  $G_c$  is the concrete elastic shear modulus and  $\beta$  is the shear retention factor. The parameter  $\beta$  is defined as a constant value or as a function of the current crack normal strain,  $\varepsilon_n^{cr}$ , and of the ultimate crack normal strain,  $\varepsilon_{n,u}^{cr}$ , as follows,

$$\beta = \left( 1 - \frac{\varepsilon_n^{cr}}{\varepsilon_{n,u}^{cr}} \right)^{p_1} \quad (15)$$

when  $p_1 = 1$ , a linear decrease of  $\beta$  with the increase of  $\varepsilon_n^{cr}$  is assumed. Larger values of the exponent  $p_1$  correspond to a more pronounced decrease of the  $\beta$  parameter [4].

In structures governed by flexural failure modes, this strategy leads to simulations with reasonable accuracy. Exceptions occur in structures that fail by the formation of a critical shear crack. To simulate accurately the deformational response and the crack pattern up to the failure of this type of structures, the adoption of a softening crack shear stress vs. crack shear strain relationship ( $\tau_t^{cr} - \gamma_t^{cr}$ ) is the strategy explored in the present work.

The crack shear stress vs. shear strain diagram represented in Figure 2 was adopted in the simulations performed in the present work, but other more sophisticated diagrams were also implemented in FEMIX computer program, and their corresponding formulations are described in detailed elsewhere [6].

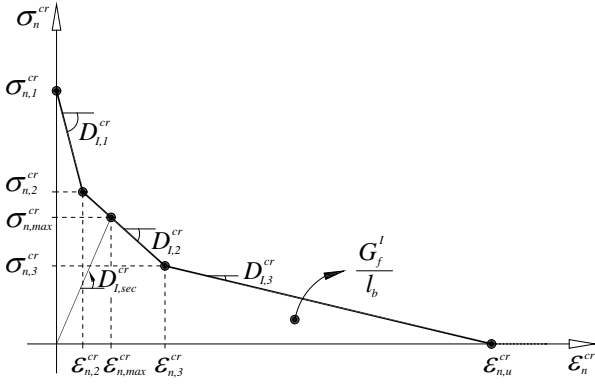


**Figure 1:** Trilinear stress-strain diagram to simulate the fracture mode I crack propagation ( $\sigma_{n,2}^{cr} = \alpha_1 \sigma_{n,1}^{cr}$ ,  $\sigma_{n,3}^{cr} = \alpha_2 \sigma_{n,1}^{cr}$ ,  $\epsilon_{n,2}^{cr} = \xi_1 \epsilon_{n,u}^{cr}$ ,  $\epsilon_{n,3}^{cr} = \xi_2 \epsilon_{n,u}^{cr}$ ).

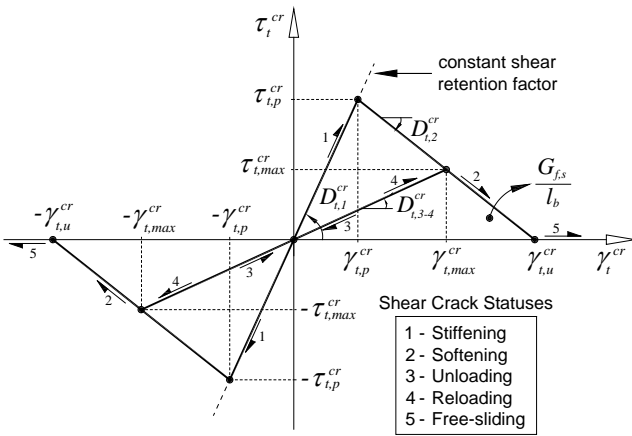


**Figure 2:** Diagram to simulate the relationship between the crack shear stress and crack shear strain component, and possible shear crack statuses.

According to the adopted approach for modelling the crack shear deformation,  $\tau_t^{cr} - \gamma_t^{cr}$ , the crack shear stress increases linearly until the crack shear strength is reached,  $\tau_{t,p}^{cr}$ , (first branch of the shear crack diagram), followed by a decrease of the  $\tau_t^{cr}$  with the increase of  $\gamma_t^{cr}$  (softening branch). The diagram represented in Figure 2 is defined by the following equations:

$$\tau_t^{cr}(\gamma_t^{cr}) = \begin{cases} D_{I,1}^{cr} \gamma_t^{cr} & 0 < \gamma_t^{cr} \leq \gamma_{t,p}^{cr} \\ \tau_{t,p}^{cr} - \frac{\tau_{t,p}^{cr}}{(\gamma_{t,u}^{cr} - \gamma_{t,p}^{cr})} (\gamma_t^{cr} - \gamma_{t,p}^{cr}) & \gamma_{t,p}^{cr} < \gamma_t^{cr} \leq \gamma_{t,u}^{cr} \\ 0 & \gamma_t^{cr} > \gamma_{t,u}^{cr} \end{cases} \quad (16)$$

The initial shear fracture modulus,  $D_{I,1}^{cr}$ , is defined by equation (14) ( $D_{II}^{cr}$  is replaced by  $D_{I,1}^{cr}$ ) by assuming for  $\beta$  a constant value in the range ]0,1[. The peak crack shear strain,  $\gamma_{t,p}^{cr}$ , is obtained using the crack shear strength (from the input data),  $\tau_{t,p}^{cr}$ , and the crack shear modulus:

$$\gamma_{t,p}^{cr} = \frac{\tau_{t,p}^{cr}}{D_{I,1}^{cr}} \quad (17)$$

The ultimate crack shear strain,  $\gamma_{t,u}^{cr}$ , depends on the crack shear strength,  $\tau_{t,p}^{cr}$ , on the shear fracture energy (mode II fracture energy),  $G_{f,s}$ , and on the crack bandwidth,  $l_b$ :

$$\gamma_{t,u}^{cr} = \frac{2G_{f,s}}{\tau_{t,p}^{cr} l_b} \quad (18)$$

In the present approach it is assumed that the crack bandwidth, used to assure that the results are independent of the mesh refinement [5], is the same for both fracture mode I and mode II processes, but specific research should be done in this respect in order to assess the influence of these model parameters on the predictive performance of the behaviour of elements failing in shear.

When the softening constitutive law represented in Figure 2 is used to evaluate the fracture mode II softening modulus  $D_{II}^{cr}$  of equation (7), its value depends on the branches defining the diagram. For this reason five shear crack statuses are proposed and their meaning is schematically represented in Figure 2. The crack mode II modulus of the first linear branch of the diagram is defined by equation (14), the second linear softening branch is defined by

$$D_{II}^{cr} = D_{I,2}^{cr} = -\frac{\tau_{t,p}^{cr}}{\gamma_{t,u}^{cr} - \gamma_{t,p}^{cr}} \quad (19)$$

and the crack shear modulus of the unloading and reloading branches is obtained from

$$D_{II}^{cr} = D_{I,3-4}^{cr} = \frac{\tau_{t,max}^{cr}}{\gamma_{t,max}^{cr}} \quad (20)$$

being  $\gamma_{t,max}^{cr}$  and  $\tau_{t,max}^{cr}$  the maximum crack shear strain already attained and the corresponding crack shear stress determined

from the softening linear branch. Both components are stored to define the unloading/reloading branch (see Figure 2).

In free-sliding status,  $|\gamma_t^{cr}| > |\gamma_{t,u}^{cr}|$ , the crack mode II stiffness modulus,  $D_{II}^{cr} = D_{t,5}^{cr}$ , is null.

To avoid numerical instabilities in the calculation of the stiffness matrix, when the crack shear status is free-sliding a residual crack shear stress value is assumed for this phase of sliding.

A free-sliding status is also assigned to the shear crack status when  $\varepsilon_n^{cr} > \varepsilon_{n,u}^{cr}$ . The details about how the shear crack statuses are treated can be consulted elsewhere [6].

### 3 PREDICTIVE PERFORMANCE OF THE NUMERICAL MODEL

#### 3.1 Introduction

To assess the predictive performance of the model described in previous section, the experimental tests carried out with a series of rectangular cross section reinforced concrete (RC) beams shear strengthened according to the Embedded Through-Section (ETS) technique were simulated. According to this strengthening technique, holes are opened through the beam's section, with the desired inclinations, and bars are introduced into these holes and bonded to the concrete substrate with adhesive materials. The strengthening elements are composed of steel bars bonded to the surrounding concrete with an epoxy adhesive.

#### 3.2 Series of beams

The experimental program is formed by a series of beams with a cross section of  $150 \times 300 \text{ mm}^2$ , with a total length of 2450 mm and a shear span length of 900 mm (Figures 3 and 4). The longitudinal tensile and compressive steel reinforcement consist of two steel bars of 25 mm diameter and two steel bars of 12 mm diameter, respectively. Steel stirrups of two vertical arms and 6 mm diameter were used. The concrete clear cover for the top, bottom and lateral faces of the beams was 20 mm. The experimental program is made up of a beam without any shear reinforcement (reference beam), and a beam for each of the following shear reinforcing systems: (i) steel stirrups of  $\varnothing 6 \text{ mm}$  at a spacing of 300 mm (S300.90), (ii) ETS strengthening bars at  $90^\circ$  (E300.90) or at  $45^\circ$  (E300.45) in relation to the beam axis, with a spacing of 300 mm, (iii) steel stirrups of  $\varnothing 6 \text{ mm}$  at a spacing of 300 mm and ETS strengthening bars at  $90^\circ$  (S300.90/E300.90) or at  $45^\circ$  (S300.90/E300.45), with a spacing of 300 mm, (iv) steel stirrups of  $\varnothing 6 \text{ mm}$  at a spacing of 225 mm (S225.90), and (v) steel stirrups of  $\varnothing 6 \text{ mm}$  at a spacing of 225 mm and ETS strengthening bars at  $90^\circ$ , with a spacing of 225 mm (S225.90/E225.90). ETS bars of  $\varnothing 10 \text{ mm}$  were used.

It should be noted that an ETS bar was designed as a stirrup of one arm, following the design recommendations of ACI 318 Code [7] for the steel stirrups in the context of shear reinforcement or RC beams.

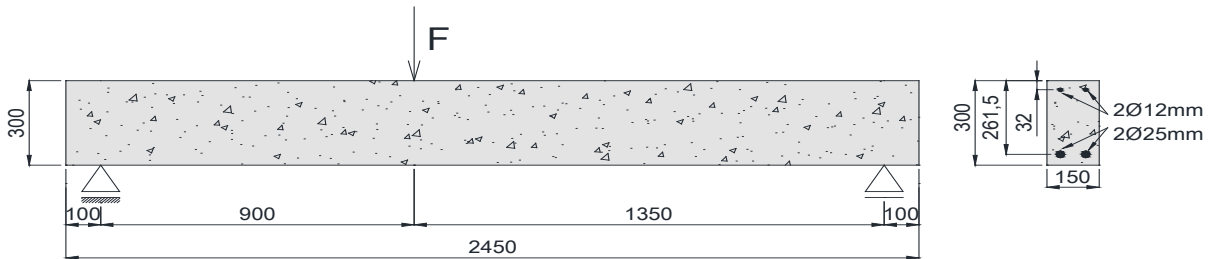


Figure 3: Test configuration. All dimensions are in mm

Beams ID	Shear strengthening system	Shear strengthening arrangements	Shear span reinforcement/strengthening
Reference	-----		
S300.90	Stirrups at 90° (2φ6 mm, 2 arms, 300 mm spacing)		
E300.90	ETS strengthening bars at 90° (3φ10 mm, 300 mm spacing)		
E300.45	ETS strengthening bars at 45° (3φ10 mm, 300 mm spacing)		
S300.90/ E300.90	Stirrups at 90° (2φ6 mm, 2 arms, 300 mm spacing) ETS strengthening bars at 90° (3φ10 mm, 300 mm spacing)		
S300.90/ E300.45	Stirrups at 90° (2φ6 mm, 2 arms, 300 mm spacing) ETS strengthening bars at 45° (3φ10 mm, 300 mm spacing)		
S225.90	Stirrups at 90° (3φ6 mm, 2 arms, 225 mm spacing)		
S225.90/ E225.90	Stirrups at 90° (3φ6 mm, 2 arms, 225 mm spacing) ETS strengthening bars at 90° (4φ10 mm, 225 mm spacing)		

Figure 4: General information about the beams of the experimental program

### 3.3 Test setup and monitoring system

Figure 5 depicts the positioning of the sensors for data acquisition. To measure the deflection of a beam, four linear voltage differential transducers (LVDTs) were supported in a suspension yoke. The LVDT 3558 was also used to control the tests at a displacement rate of  $20 \mu\text{m/s}$  up to the failure of the beams. The beams were loaded under three-point bending with a shear span of 900 mm. This corresponded to an  $a/d$  ratio equal to 3.44, where  $a$  is the shear span and  $d$  the depth of the longitudinal reinforcement (Figure 3). The applied load ( $F$ ) was measured using a load cell of  $\pm 500 \text{ kN}$  and accuracy of  $\pm 0.05\%$ . Two or three electrical resistance strain gauges, depending on the shear reinforcing arrangement, were installed in the steel stirrups to measure the strains. Additionally, six or eight strain gauges, SGs, were bonded on the ETS strengthening bars according to the strengthening arrangement represented in Figure 4.

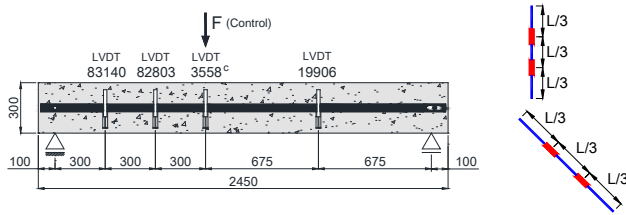


Figure 5: Monitoring system.

### 3.4 Material properties

The values for the characterization of the main properties of the materials used in the present work were obtained from experimental tests and can be found elsewhere [3].

### 3.5 Main results

Figure 6 shows the relationship between the total applied load and the deflection of the loaded section,  $F-u$ , of the beams. For similar shear reinforcement ratio and ETS strengthening ratio the RC beams reinforced with steel stirrups or strengthened with ETS bars have identical behavior (S300.90 and E300.90 beams). For the beams with ETS bars of equal spacing but different inclination (which means different shear strengthening ratio), ETS bars applied at

45-degrees have provided a higher increase in terms of load carrying capacity and deflection at peak load (E300.90 versus E300.45 beams). Due to the significant increase provided by the ETS bars for the shear resistance, the beams reinforced with steel stirrups and strengthened with ETS bars collapsed by the yielding of the longitudinal steel bars, followed by concrete crushing.

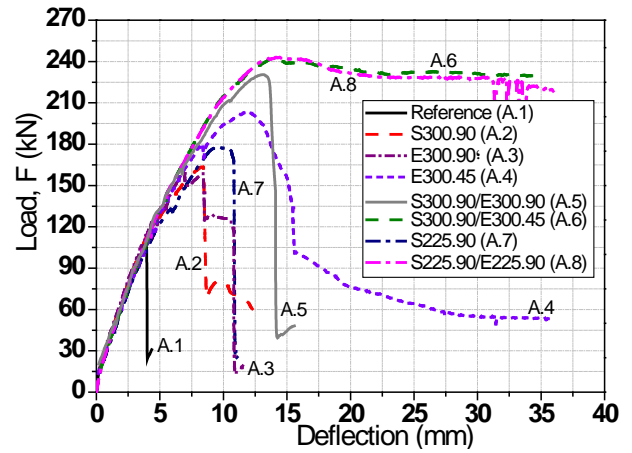


Figure 6: Relationship between the load and the deflection at the loaded section.

### 3.6 Finite element mesh, integration schemes and constitutive laws for the materials

To simulate the crack initiation and the fracture mode I propagation of reinforced concrete, the trilinear tension-softening diagram represented in Figure 1 was adopted. To distinguish concrete elements in tension softening and in tension stiffening, distinct values were considered for the concrete of the elements in the first two rows of finite element mesh (elements considered in tension stiffening). The values that define these diagrams are indicated in Table 1. In this table is also included the data necessary to define the shear-softening diagram represented in Figure 2, adopted to simulate the degradation of crack shear stress transfer after crack initiation. Since no available experimental results exist to characterize the crack shear softening diagram, the adopted values were obtained by inverse analysis by fitting the experimental results as best as possible.

An example of a finite element mesh used for the simulation of the S225.90/E225.90 beam is represented in Figure 7. The beams are modelled with a mesh of 8-noded serendipity plane stress finite elements. A Gauss-Legendre integration scheme with  $3 \times 3$  IP is used in all

concrete elements. The longitudinal steel bars, stirrups and the ETS strengthening bars are modelled with 3-noded perfect bonded embedded cables (one degree-of-freedom per each node) and a Gauss-Legendre integration scheme with 3 IP (integration point) is used.

**Table 1:** Values of the parameters of the concrete constitutive model

Poisson's ratio ( $\nu_c$ )	0.15
Initial Young's modulus ( $E_c$ )	31100 N/mm <sup>2</sup> (Batch 1) 30590 N/mm <sup>2</sup> (Batch 2)
Compressive strength ( $f_c$ )	30.78 N/mm <sup>2</sup> (Batch 1) 28.81 N/mm <sup>2</sup> (Batch 2)
Trilinear tension-stiffening diagram <sup>(1)</sup>	$f_{ct} = 2.0$ N/mm <sup>2</sup> ; $G_f = 0.06$ N/mm $\xi_1 = 0.01$ ; $\alpha_1 = 0.5$ ; $\xi_2 = 0.5$ ; $\alpha_2 = 0.2$
Trilinear tension-softening diagram <sup>(1)</sup>	$f_{ct} = 1.8$ N/mm <sup>2</sup> ; $G_f = 0.05$ N/mm $\xi_1 = 0.01$ ; $\alpha_1 = 0.4$ ; $\xi_2 = 0.5$ ; $\alpha_2 = 0.2$
Parameter defining the mode I fracture energy available to the new crack [4]	$n = 2$
Parameters for defining the softening crack shear stress-shear strain diagram of concrete in the tension-stiffening	$\tau_{t,p}^{cr} = 1.38$ N/mm <sup>2</sup> ; $G_{f,s} = 0.5$ N/mm; $\beta = 0.2$
Parameters for defining the softening crack shear stress-shear strain diagram of concrete in the tension-softening	$\tau_{t,p}^{cr} = 1.38$ N/mm <sup>2</sup> ; $G_{f,s} = 0.7$ N/mm; $\beta = 0.2$
Crack bandwidth, $l_b$	Square root of the area of Gauss integration point
Threshold angle [4]	$\alpha_{th} = 30^\circ$
Maximum number of cracks per integration point	2

<sup>(1)</sup>  $f_{ct} = \sigma_{n,1}^{cr}$ ;  $\xi_1 = \varepsilon_{n,2}^{cr} / \varepsilon_{n,u}^{cr}$ ;  $\alpha_1 = \sigma_{n,2}^{cr} / \sigma_{n,1}^{cr}$ ;  $\xi_2 = \varepsilon_{n,3}^{cr} / \varepsilon_{n,u}^{cr}$ ;  $\alpha_2 = \sigma_{n,3}^{cr} / \sigma_{n,1}^{cr}$  (see Figure 1)

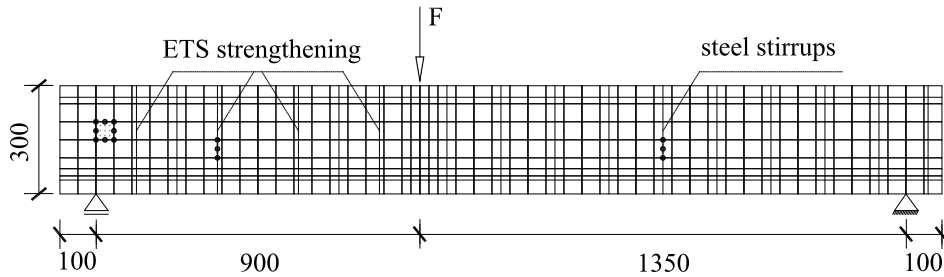


**Figure 7:** Finite element mesh (dimensions are in mm)

For modeling the behavior of the longitudinal steel bars, stirrups and ETS bars, the stress-strain relationship represented in Figure 8 was adopted. The curve (under compressive or tensile loading) is defined by the points  $PT1=(\varepsilon_{sy}, \sigma_{sy})$ ,  $PT2=(\varepsilon_{sh}, \sigma_{sh})$  and  $PT3=(\varepsilon_{su}, \sigma_{su})$ , and a parameter  $p$  that defines the shape of the last branch of the curve. Unloading and reloading linear branches with

slope  $E_s = (\sigma_{sy} / \varepsilon_{sy})$  are assumed in the present approach. The values of the parameters of the constitutive model for the steel are indicated in Table 2.

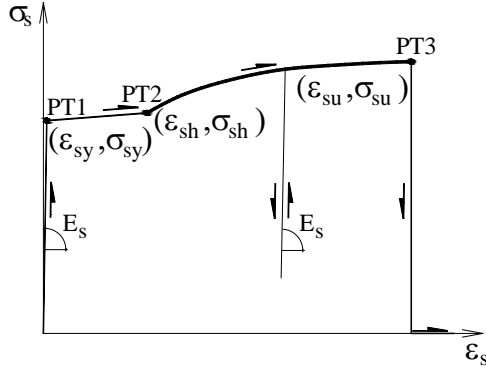


**Figure 8:** Uniaxial constitutive model for the steel bars [4].

**Table 2:** Values of the parameters of the steel constitutive model.

Steel bar diameter (mm)	PT1	PT2	PT3	$p$
	$\varepsilon_{sy} [-]$ $\sigma_{sy} (MPa)$	$\varepsilon_{sh} [-]$ $\sigma_{sh} (MPa)$	$\varepsilon_{su} [-]$ $\sigma_{su} (MPa)$	
6	$2.750 \times 10^{-3}$ 559.14	$2.000 \times 10^{-2}$ 708.14	$5.000 \times 10^{-2}$ 708.93	1
10	$2.660 \times 10^{-3}$ 541.60	$2.405 \times 10^{-2}$ 643.23	$5.000 \times 10^{-2}$ 643.23	1
12	$2.350 \times 10^{-3}$ 484.68	$2.302 \times 10^{-2}$ 655.00	$5.000 \times 10^{-2}$ 655.53	1
25	$2.270 \times 10^{-3}$ 507.68	$3.450 \times 10^{-3}$ 608.75	$2.052 \times 10^{-2}$ 743.41	1

### 3.7 Simulations and discussion

The experimental and the numerical relationships between the applied load and the deflection at the loaded section for the tested beams are compared in Figure 9. In these figures a horizontal line corresponding to the maximum experimental load (in dash) is also included. The crack patterns of these beams at the end of the analysis (at the end of the last converged load increment) are represented in Figure 10.

These figures show that the numerical model is able to capture with good accuracy the deformational response of the beams and captured with good precision the localization and profile of the shear failure crack. Figure 11 also shows that the numerical simulations fit with good accuracy the strains measured in the steel stirrups and ETS strengthening bars, which means that the assumption of perfect bond between composite materials and

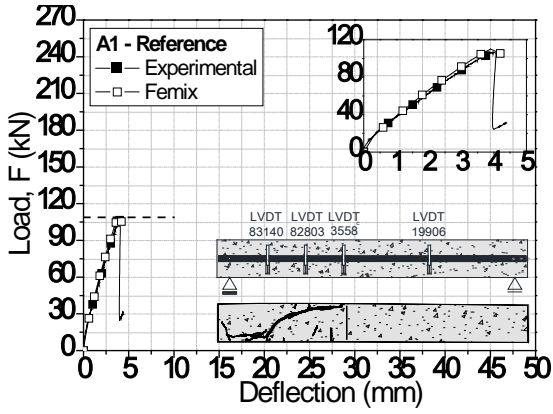
surrounding concrete is acceptable, at least in the design point of view for the serviceability and ultimate limit states. Similar level of accuracy was obtained in the simulations of the other beams. At the moment of the shear failure, the longitudinal steel bars have already yielded in some of the beams, which is quite well predicted by the numerical models, since vertical completely open cracks were formed (flexural cracks).

## 4 CONCLUSION

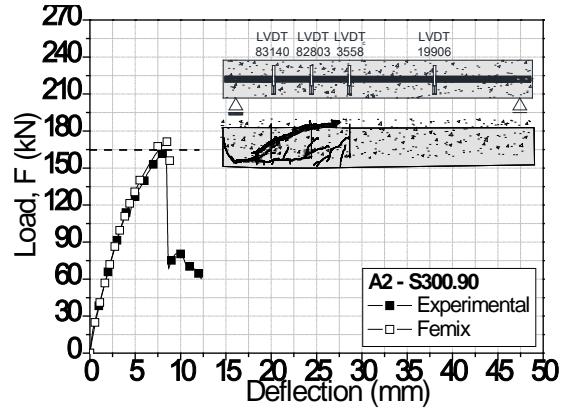
This study presents the relevant results of an experimental program for the assessment of the effectiveness of the Embedded Through-Section (ETS) technique for the shear strengthening of reinforced concrete beams. From the obtained results, it can be concluded that:

1) the use of steel ETS bars for the shear strengthening provided significant increase of the load carrying capacity of RC beams for the both bar orientations considered. The effectiveness is also significant in terms of the deflection performance. The shear reinforcement system composed by inclined ETS strengthening bars was more effective than vertical ETS bars, assuring a better performance in terms of load and deflection capacities.

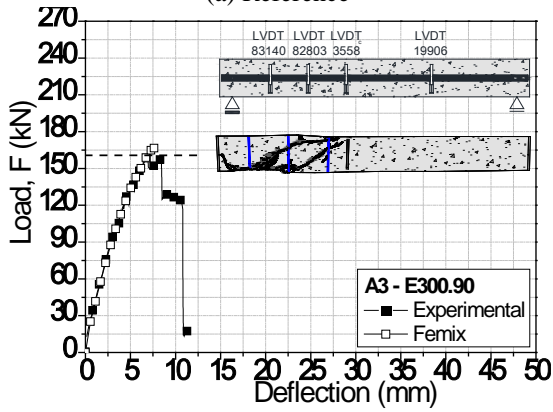
2) the capability of a FEM-based computer program to predict with high accuracy the behavior of this type of structures up to its collapse was highlighted. The introduction of the shear crack softening diagram into the multi-directional fixed smeared crack model has improved significantly the deformational behavior and the load carrying capacity. The crack pattern of the tested beams and the strain fields in the reinforcements were also captured with high accuracy. Due to the lack of specific experimental tests, the data to define the shear crack softening diagram was obtained by inverse analysis. It can be concluded that the implementation of the shear softening diagram in the multi-directional fixed smeared crack model available in the FEMIX computer program has improved its capabilities to predict with higher accuracy the behavior of structures failing in shear or in flexural/shear.



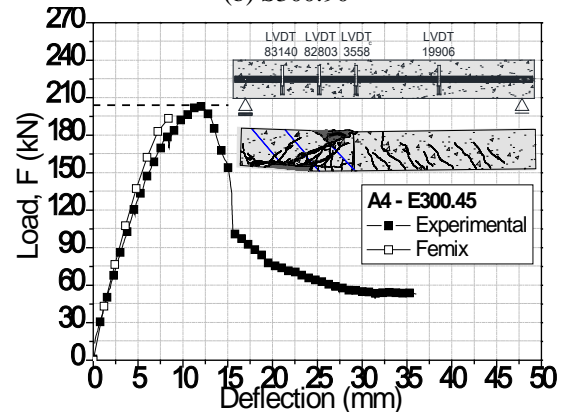
(a) Reference



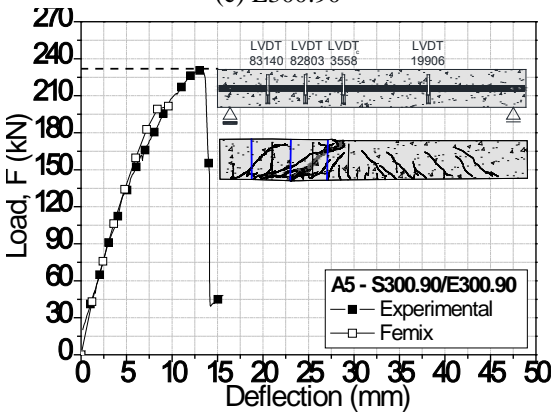
(b) S300.90



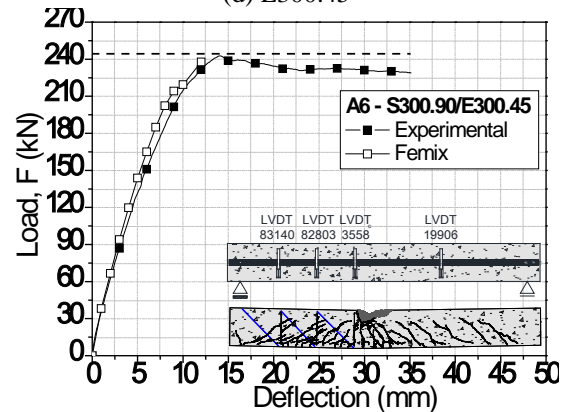
(c) E300.90



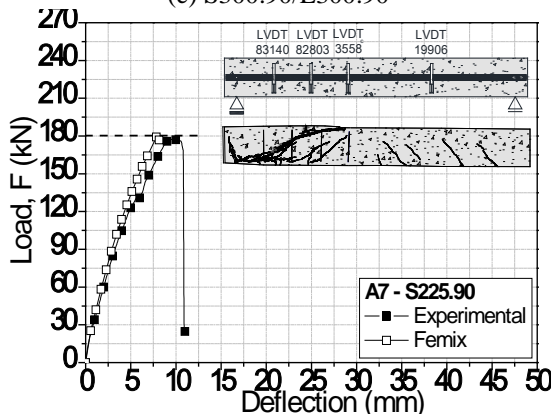
(d) E300.45



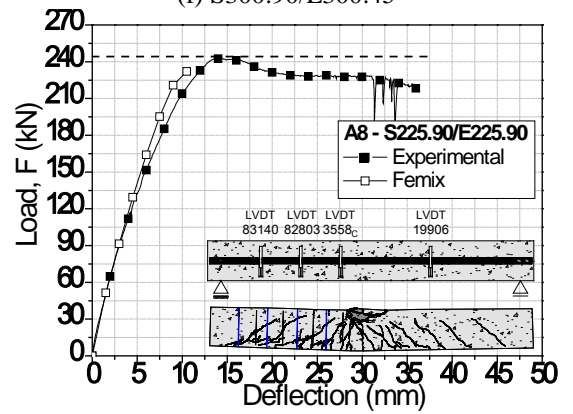
(e) S300.90/E300.90



(f) S300.90/E300.45



(g) S225.90



(h) S225.90/E225.90

Figure 9: Load-deflection at the loaded section

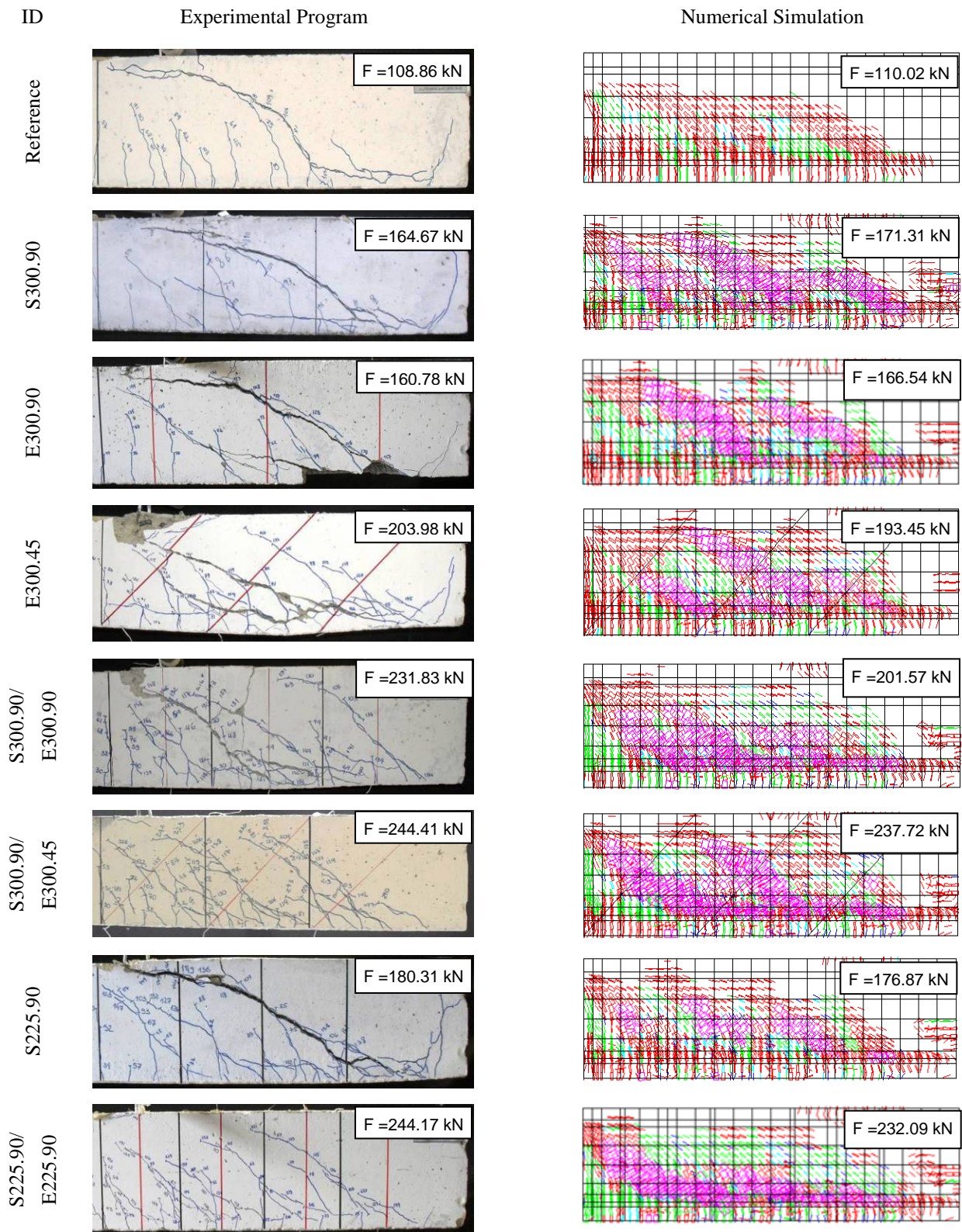


**Figure 10:** Crack patterns of the beams (in pink colour: crack completely open; in red colour: crack in the opening process; in cyan colour: crack in the reopening process).

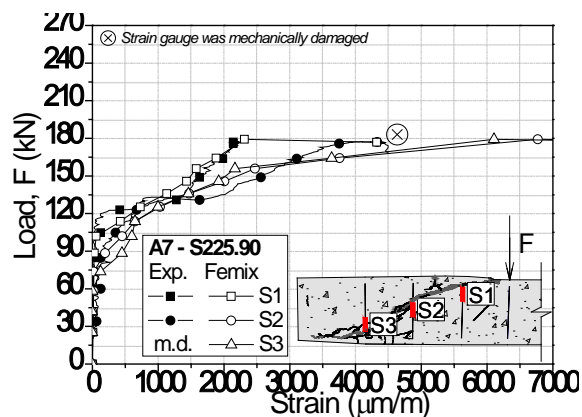
## 5 ACKNOWLEDGEMENTS

The study presented in this paper is part of the research project titled “DURCOST - Innovation in reinforcing systems for sustainable pre-fabricated structures of higher durability and enhanced structural performance” with reference number of PTDC/ECM/105700/2008. The authors also thank the collaboration of the following companies: Casais to manufacture the moulds, Secil/Unibetão for providing the concrete, SIKA for supplying the superplasticizers adhesives; CiviTest for the collaboration on the strengthening procedures.

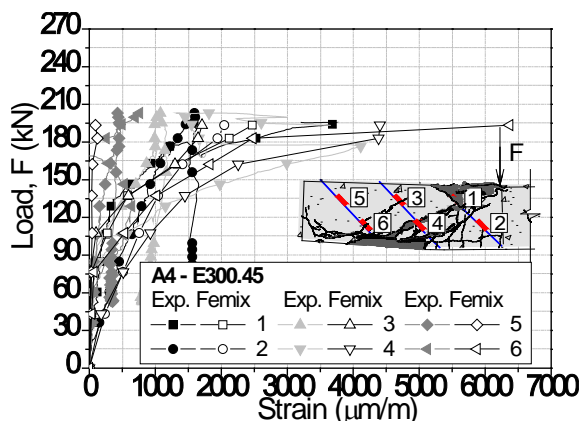
## REFERENCES

- [1] Rots, J.G. and de Borst, R., 1987. Analysis of mixed-mode fracture in concrete. *Journal of Engineering Mechanics-ASCE*, 113(11): 1739-1758.
- [2] Barros, J.A.O., Costa, I. G. and Ventura-Gouveia, A., 2011. CFRP flexural and shear strengthening technique for RC beams: experimental and numerical research. *Advances in Structural Engineering Journal*, 14(3), 559-581.
- [3] Barros, J.A.O. and Dalfré, G.M., 2012. Assessment of the effectiveness of the embedded through-section technique for the shear strengthening of RC beams. Accepted to be published in the *Strain International Journal*.
- [4] Sena-Cruz, J.M, 2004. Strengthening of concrete structures with near-surface mounted CFRP laminate strips. *PhD Thesis*, Department of Civil Engineering, University of Minho. <http://www.civil.uminho.pt/composites>.
- [5] Rots, J.G., 1988. Computational modeling of concrete fracture. *PhD Thesis*, Delft University of Technology.
- [6] Ventura-Gouveia, A., 2011. Constitutive models for the material nonlinear analysis of concrete structures including time dependent effects. *PhD Thesis*, University of Minho.

- [7] ACI Committee 318, 2008. Building code requirements for structural concrete and Commentary (ACI 318-08). Committee 318, *American Concrete Institute*, Detroit.



(a)



(b)

**Figure 11** - Load vs. strains in the shear reinforcement of the beams: (a) S225.90, and (b) E300.45